

# Data Mining of MR Technical Parameters: A Case Study for SAR in a Large- Scale MR Repository

Adriana Murraças, University of Aveiro, Portugal

Paula Maria Vaz Martins, School of Health Sciences, University of Aveiro, Portugal

Carlos Daniel Cipriani Ferreira, Perspectum Diagnostics, Ltd, Oxford, UK & Institute of Nuclear Sciences Applied to Health (ICNAS), University of Coimbra, Portugal

Tiago Marques Godinho, University of Aveiro, Portugal

Augusto Marques Ferreira da Silva, University of Aveiro, Portugal

## ABSTRACT

Exposure to radiofrequency (RF) energy during a magnetic resonance imaging exam is a safety concern related to biological thermal effects. Estimation of the specific absorption rate (SAR) is done by manufacturer scanner integrated tools to monitor RF energy. This work presents an exploratory approach of DICOM metadata focused in whole-body SAR values, patient dependent parameters, and pulse sequences. Previously acquired abdominopelvic and head studies were retrieved from a 3 Tesla scanner. Dicoogle tool was used for metadata indexing, mining, and extraction. Specifically weighted pulse sequences were related with weight, BMI, and gender through boxplot diagrams and effect size analysis. A decrease of SAR values with increasing body weight and BMI categories is observable for abdominopelvic studies. Head studies showed different trends regarding distinct pulse sequences; in addition, underage patients register higher SAR values compared to adults. Male individuals register marginally higher SAR values. Metadata recording practices and standardization need to be improved.

## KEYWORDS

Cliff's Delta, Data Mining, Dicoogle, Effect Size, Large Repository, Magnetic Resonance, Pulse Sequences, Specific Absorption Rate

## INTRODUCTION

The imaging modality of magnetic resonance (MR) involves the absorption of radiofrequency (RF) energy by the human body, comprising one of the main patient safety concerns during the exam due to heating risk of tissues. Monitoring RF absorption is achieved by the estimation of specific absorption rate (SAR) expressed in watts per kilogram (W/kg) (Hartwig, 2015).

Several studies deal with SAR values over computational simulations, but the usage of the ones obtained in real patient in everyday MR practice are hardly ever analyzed. Guidelines and reviews address SAR as dependent of the patient weight, introduced by the MR technologist, but are not specific in what way weight influences SAR. The only way to assess SAR during the MR exam is to trust in the methods applied by the manufacturers, that return an output of an estimated SAR that can limit acquisition conditions according to guideline values.

DOI: 10.4018/IJEHMC.2021010102

This article, published as an Open Access article on January 7, 2021 in the gold Open Access journal, International Journal of E-Health and Medical Communications (converted to gold Open Access January 1, 2021), is distributed under the terms of the Creative Commons Attribution License (<http://creativecommons.org/licenses/by/4.0/>) which permits unrestricted use, distribution, and production in any medium, provided the author of the original work and original publication source are properly credited.

In this respect, the scope of this article is to present an exploratory approach of whole-body SAR values reported by the equipment and stored in DICOM metadata. It uses a large metadata repository acquired in a 3 Tesla scanner. Such repository was indexed in an open source platform named Dicoogle. Data was organized, selected, and characterized. Abdominopelvic and head studies were selected for further analysis as well as specifically weighted pulse sequences for each study type. Whole-body SAR values were related with categorical patient weight, categorical BMI, and sex. This study also deals with statistical analysis regarding large data repositories.

The objectives of this work are, on one hand, related with SAR values and, on the other hand, with data itself. Specifically, assess the scenario regarding whole-body SAR values reported by the MR scanner and acquired in real patients, looking for trends or patterns regarding human physical factors (patient weight, BMI, and sex) and image acquisition parameters (pulse sequences). Simultaneously, dealing with a large repository of MR metadata, given its specific constraints such as data handling, data diversity, and data statistical analysis.

This article is organized as follows. The Background section includes the presentation of the problem, related nomenclature and reference to relevant literature on the topic. Section of Methods describes the applied approach, including a flowchart, regarding three separated topics: Data acquisition, organization, and preparation; Data characterization; and Data representation and statistical analysis. Section of Results is divided into three matters: Weight and BMI: abdominopelvic studies; Weight and BMI: head studies; and Sex: abdominopelvic and head studies. Discussion section examines the observed results, referring to comparative literature when reasonable. Ending with Conclusion section, where the main findings, limitations and future scope are addressed.

## BACKGROUND

Magnetic resonance (MR) is a widely used imaging modality with superior soft tissue contrast and flexible tools for diagnosis, physiological, and functional applications (Kim & Kim, 2017; Kraff & Ladd, 2016). In Europe, for the countries for which data is available, there was a general increase between 2011 and 2016 in the number of MR scans conducted relative to population size (Eurostat, 2019).

MR image acquisition does not use ionizing radiation and comprises an interaction between three types of magnetic fields with the human body: a high static magnetic field ( $B_0$ ), three gradient magnetic fields ( $G_x$ ,  $G_y$ , and  $G_z$ ), and a radiofrequency (RF) field ( $B_1$ ) (Hartwig, 2015). The timing of application of gradients and RF pulses is determined in a MR pulse sequence (pSq). There are two fundamental types of MR pSq: spin echo (SE) and gradient echo (GRE); other MR sequences are variations of these, with different parameters added on (Bitar et al., 2006). MR is considered a safe technology but is not hazard-free.

The magnetic fields involved in image acquisition can cause dangerous biological effects for the patient if the hazards are not taken into consideration (Hartwig, 2015; Stralka & Bottomley, 2007). Specifically, the RF power deposition is linked with thermal effects, due to tissue heating caused by direct absorption of energy and induced currents. The safety aspects regarding RF exposure are regulated via international government and industry guidelines published by ICNIRP (International Commission on Non-Ionizing Radiation Protection, 2014), FDA (Food and Drug Administration, 2014), and the IEC (International Electrotechnical Commission), ensuring patient safety and compliance with safe exposure levels (Hartwig, 2015). In the IEC standard, whole-body SAR limits are specified for the three MR operating modes: normal ( $< 2$  W/kg), 1<sup>st</sup> level controlled ( $< 4$  W/Kg) and 2<sup>nd</sup> level controlled ( $> 4$  W/kg). Other SAR limits are defined for different body regions and for localized SAR estimations (Fiedler, Ladd, & Bitz, 2018).

Monitoring RF energy absorption is achieved by estimation of the specific absorption rate (SAR), measured in watts per kilogram (W/kg). SAR is used in safety standards and guidelines and represents a convenient and current way to control possible temperature increases (Formica & Silvestri, 2004;

Hartwig, 2015; Kraff & Ladd, 2016). In human subjects, estimates of SAR levels are not trivial because body SAR is influenced by several variables such as type of RF pulse, repetition time, configuration of anatomic area exposed, among others (Formica & Silvestri, 2004; Shellock & Crues, 2004). MR scanners can provide an estimate of SAR by using the energy deposited by a RF pulse as a function of the patient's weight, inserted by the operator before starting the exam, and data on the transmit coil coverage to compute the global average SAR. Continuous computation is used to ensure that SAR values are within guideline limits (Hartwig, 2015; Tsai, Grant, Morteale, Kung, & Smith, 2015). Implementation of SAR estimates and guidelines lies on equipment manufacturers (Bottomley, 2008). Clinical MR scanners estimate SAR based on proprietary calculations that involve patient data entries by the MR technologist (Bottomley, 2008; Qian, El-Sharkawy, Bottomley, & Edelstein, 2013).

DICOM (Digital Imaging and Communications in Medicine) is the standard for the communication and management of medical imaging information and related data. DICOM uses specific nomenclature based on a model of the real-world called the DICOM Information Model. The data of the real-world is perceived as a DICOM object with respective attributes, called Information Object Definition (IOD). An IOD can be perceived as a collection of descriptive attributes. The list that collects all attributes is the DICOM Data Dictionary, ensuring consistency in attribute naming, formatting and processing. Each attribute is associated with a unique numeric tag. The MR image constitutes an IOD, where some attributes are common with other imaging modalities, such as the ones related to PatientID, and other are MR specific attributes. Due to the DICOM standard, after image acquisition, whole-body SAR values remain stored as metadata in the DICOM tag (0018,1316), as well as other technical and image descriptors (National Electrical Manufacturers Association, 2019; Pianykh, 2012). Another important concept related with the DICOM standard is PACS (Picture Archiving and Communication Systems). PACS are medical systems which provide storage, retrieval, management, distribution and presentation of medical images. The universal format for PACS communication is DICOM, guarantying interoperability (Pianykh, 2012). A software named Dicoogle was used in this work to manage and extract metadata. Dicoogle works as a PACS archive and is DICOM conformant, incorporating a new way to store and retrieve metadata, specially in cases of large-scale imaging studies that require DICOM tagged information (Costa et al., 2011).

A search of the existing literature revealed few studies that deal with real patient and equipment calculated SAR values, trusting the methods implemented by manufacturers, which are, in fact, the ones used in everyday clinical practice, relying on SAR to supervise RF transmission power (Kraff & Ladd, 2016). Most of the academic studies evaluate SAR using theoretical or experimental dosimetry. Numerical methods using computational simulations on human models to calculate SAR, e.g., the FDTD (finite difference time domain) method, are a focus of research in this field (Cao, Park, Cho, & Collins, 2015; Hartwig, 2015; Hartwig et al., 2013). Direct comparison between pSq with well-defined acquisition parameters and under strict conditions or testing new pSq to achieve SAR reduction are also previous research approaches (Conil, Hadjem, Lacroux, Wong, & Wiart, 2008; Malik et al., 2015; Shah, Kaffanke, & Romanzetti, 2009; Srinivasan et al., 2016; Wang & Collins, 2010). Temperature changes can be influenced by the weight input in the MR system (Ono et al., 2019) and SAR can reveal intrasubject variability (Meliadò, van den Berg, Luijten, & Raaijmakers, 2019). In addition, there is a gap in knowledge regarding the interrelations of the equipment reported whole-body SAR values with patient specific parameters such as weight or body mass index (BMI) and image acquisition parameters.

Given the scenario, this work presents itself as an exploratory approach of equipment reported whole-body SAR values stored in DICOM metadata. The use of a large repository enabled the consideration of adequate statistical methods that ask for a dedicated clarification. To perform data representation, boxplot diagrams were chosen. Patient weight is divided into six categories (M1 to M6), patient BMI into four categories (BMI1 to BMI4) and female and male sex categories. Specific methods to assess the statistical difference between categories in large samples were studied. For example, a non-parametric hypothesis test approach was tested, providing a p-value and classification

as significant or non-significant. However, statistical significance turns out to be limited information in a dataset that by its dimension assures significance, i.e., the p-value can be made small by increasing the sample size (Kalinowski & Fidler, 2010). An alternative non-parametric measure called Cliff's delta ( $\delta$ ), was calculated and used to inform the magnitude of the difference between two groups of observations. This is called a measure of effect size, that provides the magnitude of the effect and is less biased toward sample size. Effect size is more reliable in a large sample dataset, where the probability of finding a statistically significant result increases considerably (Khalilzadeh & Tasci, 2017; Macbeth, Razumiejczyk, & Ledesma, 2011). In this work, the Cliff's delta measure of effect size is calculated to all paired groups in weight, BMI and sex categories for each MR pulse sequence.

## METHODS

The following paragraphs describe the applied methodology. A summary flowchart can be found in Figure 1.

### Data Acquisition, Organization, and Preparation

A repository of previously acquired MR images of a 3T scanner with high-performance gradients (maximum amplitude, 45 mT/m; rise time, 200  $\mu$ s; slew rate, 200 T/m/s; FOV, 50 cm) was the source of the metadata. A remote installation of Dicoogle software ([www.dicoogle.pt](http://www.dicoogle.pt)) was performed and connection to the repository allowed the indexing process. The Dicoogle platform enabled the collection of all DICOM metadata associated to each image, organizing it in a patient-study-series-image hierarchy. Following the indexing process, the extraction of metadata was performed via comma-separated value (.csv) files. Metadata extraction was performed in the Dicoogle platform, considering segmented time frames (annually) by using the Study Date DICOM tag as a filter and a selected list of extracted DICOM tags.

The .csv files were worked in Excel 2016® given the particularities of the data. The first step of this process was to import the .csv files using the Get and Transform Data tool, selecting the path of the corresponding storage folder. A connection was created to each .csv file. Using the Editing mode, a new query was added to each .csv file. Each one was imported as .csv to obtain access to its content. At this stage, an Excel query was created for each .csv file. To have all the metadata in one query, the several .csv files were combined using the Append tool, with the assurance that column organization (i.e., DICOM tags extracted) was the same for every .csv file extracted from Dicoogle. The benefit of this approach is the creation of a query with the metadata information combined without loading it to an Excel sheet since it would exceed the maximum number of rows (the same as the number of images) in a worksheet.

The Editing mode was further used in the combined query, allowing a first preview of the data, filtering and removing duplicates in the column content. Filtering was performed to assure that research mode in scanning sequence was not considered and the exclusion of blank fields in patient size tag. Metadata regarding imaged phantoms were identified and excluded. The removal of duplicates was performed on three levels, given by the DICOM tags PatientID, StudyInstanceUID, and SeriesInstanceUID, on which the population, studies, and SAR values were characterized, respectively, gathering three separate worksheets.

Once the above process was applied, some formatting actions were performed. Using Excel formulas, data was formatted for correct identification of numerical fields, with specific attention on metric units. Furthermore, four new data columns were added: categorical patient weight (kg) given the ranges  $M1 < 60$ ,  $60 \leq M2 \leq 69$ ,  $70 \leq M3 \leq 79$ ,  $80 \leq M4 \leq 89$ ,  $90 \leq M5 \leq 99$ , and  $M6 \geq 100$ ; BMI was calculated given the formula  $\text{weight}/\text{height}^2$  ( $\text{kg}/\text{m}^2$ ); patients were categorized according to BMI given the ranges  $\text{BMI1} < 18,50$ ;  $18,50 \leq \text{BMI2} \leq 24,99$ ;  $25 \leq \text{BMI3} \leq 29,99$ ; and  $30 \geq \text{BMI4}$ ; finally, a column with a more readable identification of pulse sequences was added. Excel formulas

allowed fast and automatic classification for weight and BMI values according to the above defined categories for all data rows.

## Data Characterization

The initial metadata repository consisted of 61663 series of 3620 studies regarding 3086 patients. The sample was chosen regarding the highest count of studies performed: approximately 71% were head studies and 18% were abdominopelvic studies. For each study type, specifically weighted pulse sequences were selected given the highest series count (Table 1).

## Data Representation and Statistical Analysis

MATLAB software (version R2016b, 64 bits, The MathWorks Inc., Natick, MA, USA) was used to perform the following tasks. Boxplot diagrams were used to represent the data. Each pulse sequence was characterized by three boxplots: SAR vs. patient weight category, SAR vs. BMI category, and SAR vs. sex. Effect size using Cliff's delta was calculated and classified as insignificant ( $|\delta| < 0,147$ ), small ( $0,147 \leq |\delta| < 0,33$ ), moderate ( $0,33 \leq |\delta| < 0,474$ ), and large ( $|\delta| \geq 0,474$ ) (Ma, Chen, Yang, Zhou, & Xu, 2016).

## RESULTS

The abdominopelvic sample gathered a total of 17812 series (610 patients from 658 studies) and the head sample a total of 29907 series (2130 patients from 2519 studies,).

From Table 1 it is possible to observe that collected data corresponds to a wide patient population. In the abdominopelvic studies, there are records of adult patients only, whereas head studies include under-age patients. For either study type, SAR limits were never exceeded considering guidelines for whole-body SAR up to 1<sup>st</sup> level controlled mode (4 W/kg).

### Weight and BMI: Abdominopelvic Studies

Regarding abdominopelvic studies in Figure 2, Tse<sub>T2w</sub> presents the highest mean and median, with approximately 50% of SAR records above 2 W/kg, i.e., series acquired in the 1<sup>st</sup> level controlled operating mode for whole-body SAR. The remaining pSq are found to have fewer records above that threshold.

From Figures 3 and 4, in Epi pSq, the M2 and BMI2 categories are slightly elevated compared to corresponding categories. A moderate  $\delta$  between M2/M3, M2/M4, and M2/M6 was found. The BMI2/BMI3 and BMI2/BMI4 pairs have a moderate Cliff's classification.

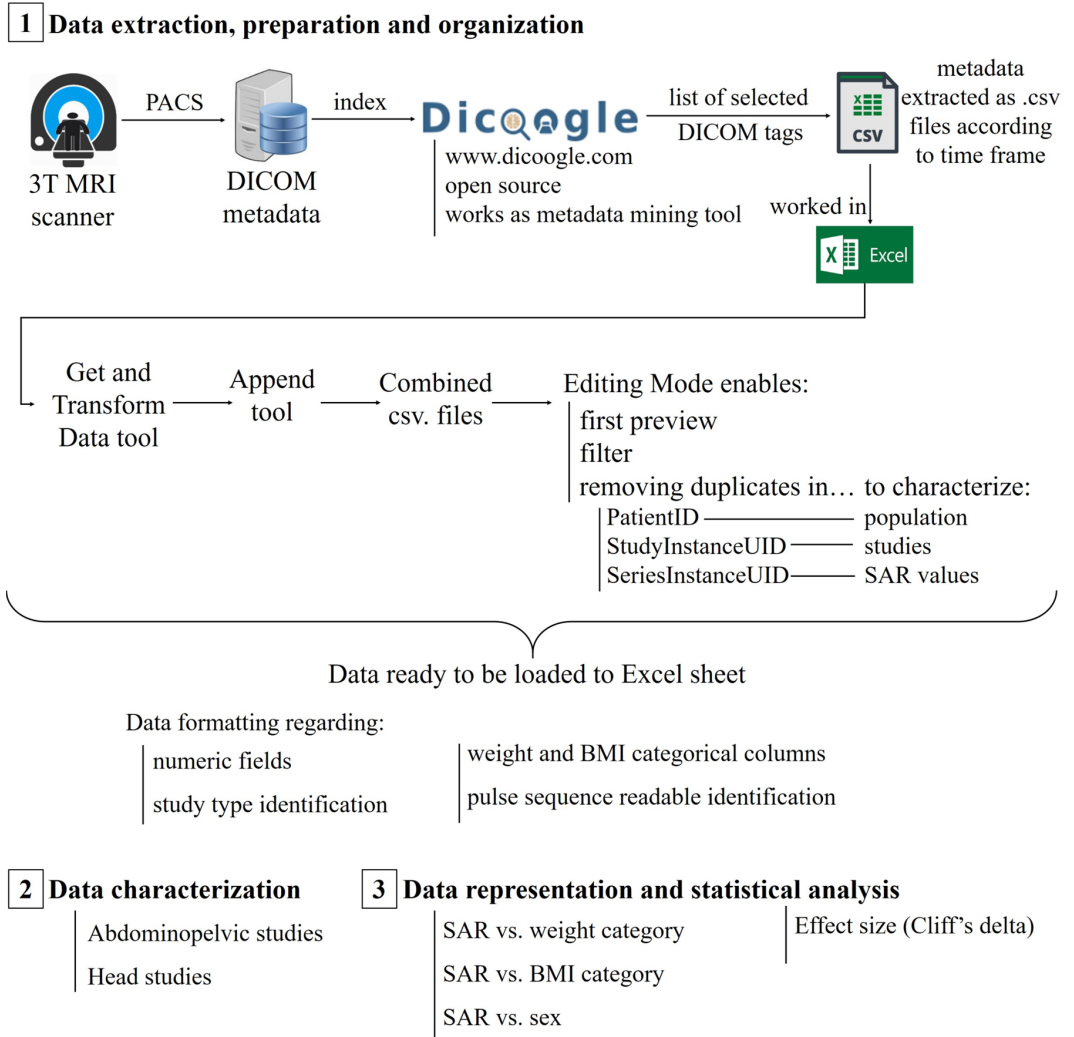
In Haste<sub>T2w</sub> pSq, the upper extreme and Q3 values decrease with increasing weight and BMI categories. A moderate  $\delta$  is found between M6 and all other weight categories. In BMI2, approximately a quarter of the records are above 2 W/kg; this value decreases in BMI3 and BMI4. A moderate  $\delta$  was found in the pair BMI2/BMI4.

Turning to SpaceR<sub>T2w</sub> pSq, box location is alike for weight and BMI categories. A large  $\delta$  was found between M2/M5 and moderate between M3/M5. In the BMI categories, values above 2W/kg are similar across all categories.

In Flash<sub>T1w</sub> pSq, the position of Q1, lower extreme, median, and mean tend to register lower values with increasing weight and BMI category (except for M6). A moderate  $\delta$  was found in M2/M4, M2/M5, and M2/M6. A  $\delta$  classified as moderate was found in BMI2/BMI4.

For Tse<sub>T2w</sub> pSq, a large range of values in the M3, M4, and M5 categories is observed. In weight and BMI categories, boxplot values tend to register progressively smaller values as category increases. Approximately half of the records are located above 2W/kg in BMI2 and BMI3, with a lower percentage in BMI4. A moderate  $\delta$  is found in BMI2/BMI4.

Figure 1. Summary flowchart of applied methodology. Three main steps highlighted: data extraction, preparation and organization; data characterization and data representation and statistical analysis.



**Weight and BMI: Head Studies**

Regarding head studies, SAR values that characterize each SqP are highly different and the existence of numerous outliers impelled the separation into two boxplot diagrams with the appropriate scale on the vertical axis. In Figure 2, SAR values recorded for head studies are mainly below the first level controlled operating mode. Tse type pSq record the highest means and medians, with a box located higher on the y-axis.

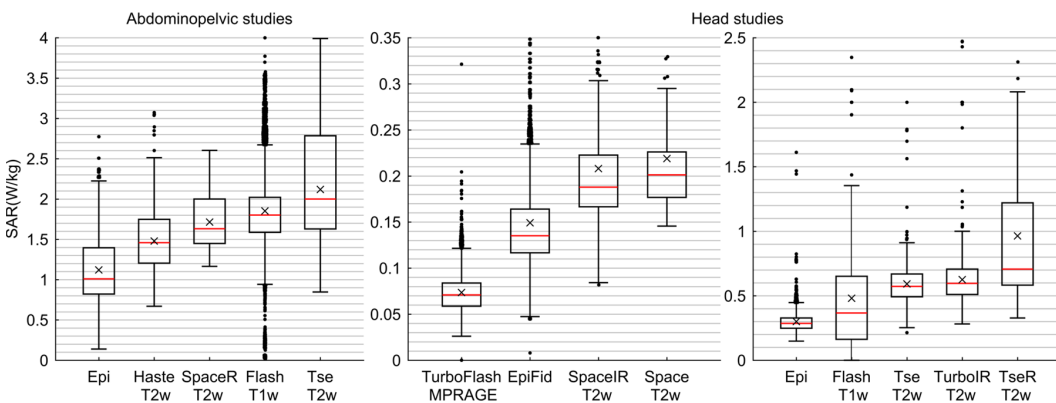
From Figures 3 and 4, in TurboFlash<sub>MPRAGE</sub> pSq it can be observed, from the M1 to M4 category, a progressively wider range of values, although box location is alike. The M6 category is located higher on the y-axis, which is confirmed with a moderate  $\delta$  between M6 and all other categories. The BMI2, BMI3 and BMI4 categories have similar box locations.

In EpiFid pSq, the M1 and BMI1 categories stand out from the remaining categories due to higher upper extreme value, Q3, and mean. This difference is confirmed with a Cliff's classification

**Table 1. Brief characterization of the demographic and technical parameters of the analyzed data for each study type (abdominopelvic and head studies)**

	Abdominopelvic studies		Head studies	
Number of series	Epi	1157	TurboFlash <sub>MPRAGE</sub>	6640
	Haste <sub>T2w</sub>	1014	EpiFid	12653
	SpaceR <sub>T2w</sub>	252	SpaceIR <sub>T2w</sub>	1120
	Flash <sub>T1w</sub>	14280	Space <sub>T2w</sub>	76
	Tse <sub>T2w</sub>	1109	Epi	3550
			Flash <sub>T1w</sub>	2066
			Tse <sub>T2w</sub>	1969
			TurboIR <sub>T2w</sub>	1527
			TseR <sub>T2w</sub>	306
	Female	2575	Female	15774
Male	15237	Male	14133	
<b>Total</b>	<b>17812</b>	<b>Total</b>	<b>29907</b>	
	<b>Mean</b>	<b>Range</b>	<b>Mean</b>	<b>Range</b>
Age (years)	62	20 – 98	46	12 days – 93
Height (meter)	1.69	1.5 – 1.92	1.67	0.5 – 1.96
Weight (kg)	81	60 – 120	76	2.5 – 115
BMI (kg/m <sup>2</sup> )	28	21 – 42	27	10 – 41
SAR (W/kg)	1.797	0.020 – 3.999	0.237	0 – 3.483

**Figure 2. SAR vs. pulse sequence boxplot for abdominopelvic (left) and head (center and right) studies sorted by ascending median**



of moderate between M1/M6, BMI1/BMI2, and BMI1/BMI4, and large between BMI1/BMI3. The M6 records a large  $\delta$  compared with the other remaining categories.

SpaceIR<sub>T2w</sub> shows that M4, M5, and BMI4 categories fall in a slightly higher mean and median. A moderate  $\delta$  is found between M3/M5, BMI2/BMI4, and BMI3/BMI4.

Regarding Space<sub>T2w</sub> pSq, the most striking result to emerge is the elevated boxes for the M1 and BMI1 categories. Observation of M2 to M5 and BMI2 to BMI4 concludes a progressively increased box position. A large  $\delta$  is found in M2/M4, M2/M5, M3/M5, and BMI2/BMI4 and a moderate  $\delta$  in M2/M3, M4/M5, BMI2/BMI3 and BMI3/BMI4.

In Epi pSq it can be noticed, once again, that the M1 and BMI1 categories are located in higher SAR values, with confirmation by a large  $\delta$  between BMI1 and remaining categories. Observing M2 to M5 and BMI3 to BMI4, the box position is alike, with the exception of M6, slightly elevated. A moderate  $\delta$  was found between M2/M6 and M5/M6 and large  $\delta$  in M3/M6.

In Flash<sub>T1w</sub> pSq, the M1 category emerges with an elevated box, confirmed with a large difference when paired to M2, M5, and M6. In the BMI categories, BMI3 records a slightly higher mean and median, but results in a small  $\delta$  when paired to BMI2 and BMI4. A moderate  $\delta$  was found in M1/M3, M2/M5, M4/M5 and M5/M6.

Tse<sub>T2w</sub> and TurboIR<sub>T2w</sub> are alike in their SAR distribution among weight and BMI categories. Differences between M1 or BMI1 and the remaining categories are confirmed with moderate or large  $\delta$  values in Tse<sub>T2w</sub> pSq.

Finally, boxes in TseR<sub>T2w</sub> pSq are in a similar range of SAR values, either in weight or BMI categories, where only small or irrelevant Cliff's classification was found between categories.

### Sex: Abdominopelvic and Head Studies

From Figure 5, the overall scenario, in either study type and respective pSq, is that SAR values tend to be slightly higher in male individuals. An exception can be found in Flash<sub>T1w</sub> pSq, where the female boxplot is slightly elevated. Regarding  $\delta$  for abdominopelvic studies, a classification of large is found in SpaceR<sub>T2w</sub> pSq, small in Flash<sub>T1w</sub> and Haste<sub>T2w</sub>, and irrelevant in Epi and Tse<sub>T2w</sub> pSq. For head studies, female/male comparisons were reported with a moderate Cliff's classification in SpaceIR<sub>T2w</sub> and Space<sub>T2w</sub>; all other pSq report a small  $\delta$ .

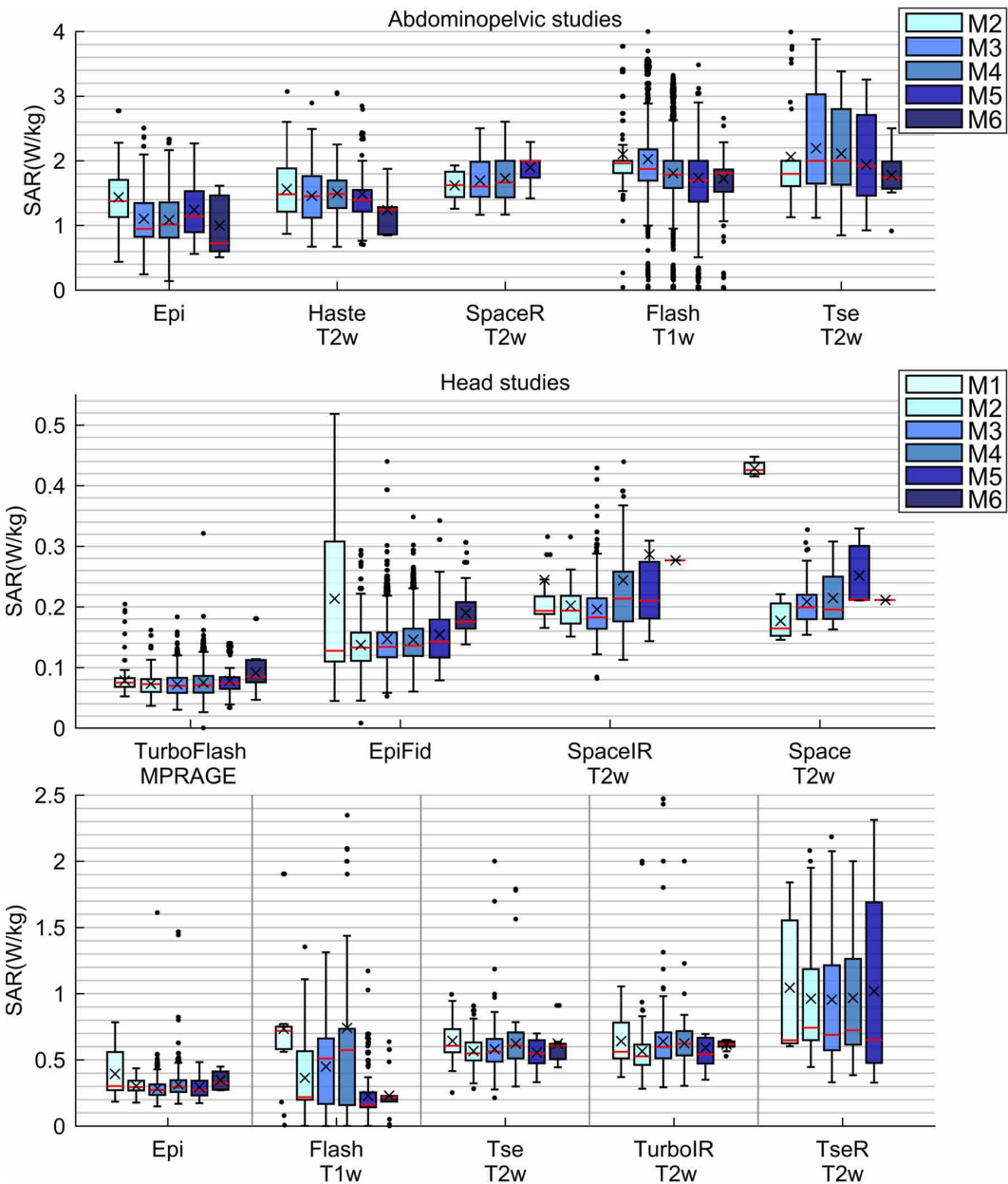
## DISCUSSION

The present work investigated the relationship between whole-body SAR values and patient specific characteristics: body weight, BMI, and sex. A large repository from a MR scanner was analyzed according to the values stored in DICOM metadata. It can be seen from the data in Table 1 that, in abdominopelvic studies, GRE pSq (Flash<sub>T1w</sub>) are used mostly to acquire T1 weighted images whereas SE pSq (Tse<sub>T2w</sub> and Haste<sub>T2w</sub>) are used to acquire T2 weighted images. This usage is consistent with routine practices in abdominal studies reported by Akisik et al. (2007). Similarly, for head studies, most T2-weighted acquisitions are performed by SE pSq (TseR<sub>T2w</sub>, TurboIR<sub>T2w</sub>, Tse<sub>T2w</sub>, Space<sub>T2w</sub>, and SpaceIR<sub>T2w</sub>), and T1 weighting by GRE pSq (Flash<sub>T1w</sub> and TurboFlash<sub>MPRAGE</sub>).

With respect to abdominopelvic studies (Figure 2), Epi pSq records the lowest median, followed by, in ascending order of median, Haste<sub>T2w</sub>, SpaceR<sub>T2w</sub>, Flash<sub>T1w</sub> and, finally, Tse<sub>T2w</sub>. Bitar et al. (2006), report that SE-type pSq, which use 90° and 180° flip angles, are associated with a higher SAR, compared to GRE pSq. In fact, we can observe from Figure 2 that Tse<sub>T2w</sub> records higher SAR values, namely half of it above 2 W/kg. However, Flash<sub>T1w</sub> appears next, with a similar position to SpaceR<sub>T2w</sub>, despite using much lower flip angles. SpaceR<sub>T2w</sub> pSq has lower SAR values compared to Tse<sub>T2w</sub> as mentioned by Nakaura et al. (2013) in a study of colon angiography and Mugler (2014), where it is stated that Space pSq allowed the reduction of SAR due to the use of variable flip angles in the refocusing pulse, being an optimized variant of a Tse pSq. In an identical scenario, head studies data from Space pSq suggest an optimized version of the Tse variants, with lower SAR values.

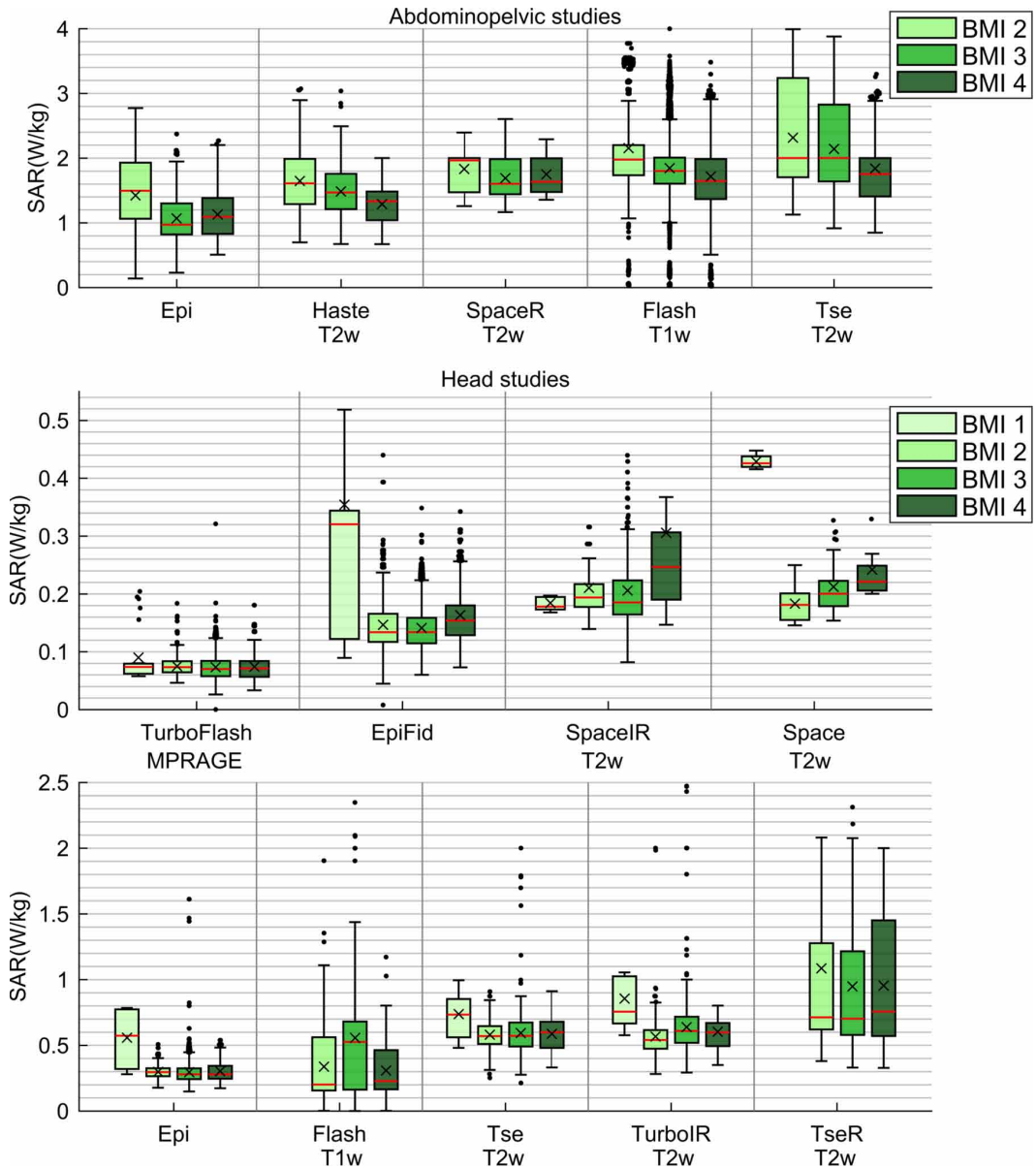
Concerning patient specific characteristics (Figures 3 and 4), observation of abdominopelvic data suggests that SAR values tend to decrease with increasing body weight and BMI category. This scenario stood out in Tse<sub>T2w</sub>, Flash<sub>T1w</sub>, and Haste<sub>T2w</sub> pSq, illustrated by a gradual decrease of upper limit, upper quartile and position of the boxplots.

Figure 3. SAR vs. weight category boxplot for abdominopelvic (top) and head (center and bottom) studies. For abdominopelvic studies in SpaceR<sub>T2w</sub> pulse sequence and for head studies in TseR<sub>T2w</sub> pulse sequence there is no data for M6 category. For head studies, SpaceIR and Space pSq register only one single value in M6, so comparison to remaining categories was not performed.



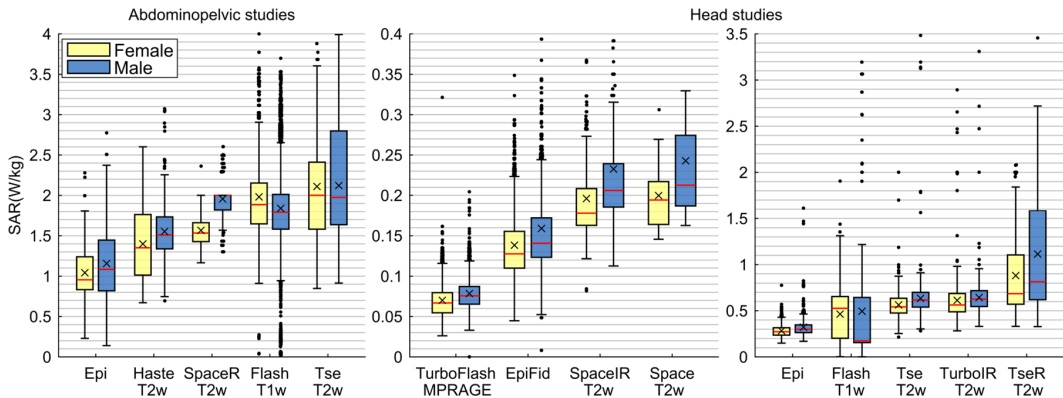
Regarding earlier findings (El-Sharkawy, Qian, Bottomley, & Edelstein, 2012), it was shown that the measured deposited power (in watts) varies linearly with BMI for a Philips MRI scanner and it is suggested that the Siemens MRI scanner model seems to depend on the subject's weight. The goal of this study was to make an independent RF power measurement to test the accuracy of scanner-reported SAR. SAR vs. weight plots are shown for each manufacturer, comparing scanner predictions and measurements, but no trends are delineated. It is possible to hypothesize that deposited

Figure 4. SAR vs. BMI category boxplot for abdominopelvic (top) and head (center and bottom) studies. For head studies in Flash<sub>T1w</sub> and TseR<sub>T2w</sub> pulse sequences there is no data for BMI1 category.



power vs. BMI linear relationship could also be found for SAR vs. BMI, since SAR is a measure to estimate RF power deposition. This trend is contrary to our findings, where SAR tends to decrease with BMI categories. In the study of Meliàdò et al. (2019), no clear relationship between BMI and the peak SAR was found. In this study, images of 23 volunteers enabled the creation of models that were used to assess intersubject and peak local SAR variability for prostate imaging at 7 T. Nevertheless, it is also referred that for higher BMI values, the worst-case peak local SAR value seems to decrease with the increase in BMI. For abdominopelvic studies, our observations confirm the scenario of the decrease of whole-body SAR values with the increase in BMI category. Meliàdò et al. refer that

Figure 5. SAR vs. sex boxplot. Illustrates the SAR distribution for female and male patients according to each pSq for abdominopelvic (left) and head (center and right) studies.



body cross-sectional area, that typically increases with weight and height of the subject, seems to influence the worst-case peak local SAR value, as this may be attributed to the increase in the average thickness of the subcutaneous fat layer in the pelvis. A similar cause might be hypothesized for our study, explaining trends of weight and BMI in abdominopelvic studies and why these trends are less visible in head studies, as the cross-sectional area could not have such a variability.

On the other hand, head studies showed different scenarios regarding distinct pulse sequences, being less certain to find a clear trend or pattern regarding SAR and body weight/BMI values. In general, SAR values in head studies are low, with most series reporting values below 1 W/kg. In head studies, M1 and BMI1 categories appear with a moderate or large Cliff's classification, representing an observable difference of these categories in comparison with the remaining. A more focused observation of the metadata realized the presence of neonates (12 to 15 days old, 6 patients, assigned as M1 and BMI1 simultaneously) and children (age below 16 years, 23 patients assigned as M1, with 4 of them assigned as BMI1). It was observed for TurboFlash<sub>MPRAGE</sub> that the outlier values between 0,155 W/kg and 0,204 W/kg (visible in both M1 and BMI1 categories) correspond to estimates for neonates. For EpiFid, in both M1 and BMI1, values between the third quartile and upper extreme value correspond to records for neonates; it also records values that are off the scale, from 0,875 W/Kg to 2,533 W/kg for the same above-mentioned population. Space<sub>T2w</sub> pSq records for M1 and BMI1 categories correspond only to neonates. For Epi, in the M1 category, values between the third quartile and the upper extreme value correspond only to neonates; similar scenario found from mean to upper extreme value in the BMI1 category. For Tse<sub>T2w</sub> pSq, the scenario is similar to Epi, but the higher records are also found in children. As described, some specific SAR values are higher in neonates or children compared to adults.

In reviewing the literature, Chavhan et al. (2009) report the experience in acquisition of MR images in children where no significant body heating was seen. On the other hand, Machata et al. (2009) report an increase of body core temperature in 3T examinations; it is suggested that the guidelines developed for awake adults may not be suited for evaluation of thermoregulation in sedated children, who may therefore be at increased possibility for clinically significant RF absorption and heating. Assuming body temperature increases are caused by RF energy deposition, SAR values should be revised to prevent hyperthermia in infants and small children. A different study (Malik et al., 2015) assessed how SAR predictions related to adults can be related to neonates. Exposure to RF energy was simulated in a neonatal anatomic model, where whole-body and head SAR was compared to adult SAR values acquired from real equipment calculations. In contrast to our findings, Malik et al. found that SAR estimates produced by an MR scanner were conservative for neonates, i.e., SAR is

lower in neonates than in adults under equivalent RF conditions. The use of neonate specific models as a mean of improving MR image quality in this population has been suggested.

In the current work, for certain pSq, neonates or children SAR values are higher compared to adults. A small sample size for children and neonates is covered so caution must be applied, and we are not confident in further extrapolation of our findings. A possible explanation for this scenario might be that SAR values are higher in child patients for safety reasons, limiting acquisition parameters, leaning on the worst-case scenario. On the other hand, the models for SAR estimation might not be suited for neonates and children anatomy.

Regarding sex (Figure 5), the general pattern is that male patients present higher SAR values compared with females, with special relevance in SpaceR<sub>T2w</sub>, Space<sub>T2w</sub>, and SpaceIR<sub>T2w</sub> due to the large and moderate Cliff classifications.

It is interesting to note that moderate and large Cliff's delta classification mostly occurs in the comparison of the most opposite categories, e.g., for abdominopelvic studies pair M2/M6 and BMI2/BMI4, and for head studies, M2/M6 and BMI1/BMI4. It seems possible that the large range of weight values enables to notice the difference between SAR values, as closely related weight categories seem to have a modest difference revealed by insignificant or small Cliff's delta.

Overall, it is possible that the findings of BMI and sex follow the pattern observed for weight: BMI is closely associated with weight, and comparison of female/male can be also associated with weight since male individuals have a higher mean body weight, resulting in higher SAR values. Therefore, body weight is a major patient related factor, if not the only one, interfering in the calculation of SAR values.

One secondary use of this metadata analysis of SAR values could be quality and safety assessment of the protocols implemented in the MR scanner, providing visualization of the variability of the SAR values, enabling a search for optimization and better practices regarding adequate protocol decision according to patient thermoregulatory conditions. In fact, it can be observed that certain pSq have a higher variability in the SAR values, namely Flash in abdominopelvic studies, and TurboFlash and EpiFid in head studies, matching the ones with the higher series count (Table 1), that is, the most performed.

The additional goal related with data handling itself presented some interesting feedback. The process of .csv extraction in Dicooogle platform was segmented in time frames because the platform was not able to extract a single .csv. for all indexed files given its computational weight. Even though the selected repository involved only one MR machine from one institution, it was possible to identify some standardization constrains, namely in study identification, pulse sequence ID, phantom ID, and other DICOM tags related to manually introduced fields. The process of identifying and excluding phantoms was time consuming since a standard denomination was not implemented. DICOM standard states that patient size units are meter but cases of values in centimeters were found. Additionally, pSq identification in PulseSequenceName DICOM tag or study type given by StudyDescription DICOM tag have different denomination for the same topic, e.g., the existence of symbols, adoption of different languages or abbreviations. This scenario indicates several limitations for analysis of a large-scale dataset, namely in the automatic classification of fields in Excel. The inconsistencies found in the metadata produced in everyday practice hinder its use for quality control of SAR limitations and for protocol optimization of MR exams. There is, therefore, a definite need for greater and better standardization in the identification of widely diverse image characteristics. The application of better data-recording practices coupled with improved automatic input to ease the usage of the produced metadata on a large scale is important to foster the encounter of imaging modalities with the recent data usage and analysis era.

## **CONCLUSION**

The findings confirm that Tse-type pSq present the highest SAR values. In addition, it is confirmed that SAR estimates are related with patient-specific characteristics, more evident in abdominopelvic studies, where SAR tends to decrease with increasing body weight and BMI category. SAR estimates for under-age patients in head studies are higher when compared to adults. This is visible in the comparison of M1 and BMI1 with the remaining categories, either in boxplot visual analysis or in Cliff's delta calculations. Limitations rely on data retrieved from only one equipment and few records on children and neonates. As future objectives, it would be interesting to analyze this work on a larger scale, with data from different institutions and equipment, as well as experimenting other software tools to ease the handling of such data. On the other hand, analyze other data sources to validate the scenario found in this work related to children and neonates. In addition, extraction and analysis of manufacturer-specific SAR metadata could provide more insight about localized SAR estimates and not only whole-body SAR that was analyzed in this work. The analysis of a large repository suggests that better practices related to manual entries of data should be implemented to assure correct estimation of patient-dependent parameters such as SAR and to promote secondary usage of everyday produced metadata.

## **ACKNOWLEDGMENT**

This research received no specific grant from any funding agency in the public, commercial, or not-for-profit sectors.

## REFERENCES

- Akisik, F. M., Sandrasegaran, K., Aisen, A. M., Lin, C., & Lall, C. (2007). Abdominal MR imaging at 3.0 T. *Radiographics*, 27(5), 1433–1444. doi:10.1148/rg.275075023 PMID:17848701
- Bitar, R., Leung, G., Perng, R., Tadros, S., Moody, A. R., Sarrazin, J., McGregor, C., Christakis, M., Symons, S., Nelson, A., & Roberts, T. P. (2006). MR pulse sequences: What Every Radiologist Wants to Know but Is Afraid to Ask. *Radiographics*, 26(2), 513–537. doi:10.1148/rg.262055063 PMID:16549614
- Bottomley, P. A. (2008). Turning Up the Heat on MRI. *Journal of the American College of Radiology*, 5(7), 853–855. doi:10.1016/j.jacr.2008.04.003 PMID:18585665
- Cao, Z., Park, J., Cho, Z.-H., & Collins, C. M. (2015). Numerical Evaluation of Image Homogeneity, Signal-to-noise Ratio, and Specific Absorption Rate for Human Brain Imaging at 1.5, 3, 7, 10.5 and 14 Tesla in an 8-channel Transmit/receive Array. *Journal of Magnetic Resonance Imaging*, 41(5), 1432–1439. doi:10.1002/jmri.24689 PMID:24976608
- Chavhan, G. B., Babyn, P. S., Singh, M., Vidarsson, L., & Shroff, M. (2009). MR imaging at 3.0 T in children: Technical differences, safety issues, and initial experience. *Radiographics*, 29(5), 1451–1466. doi:10.1148/rg.295095041 PMID:19755605
- Conil, E., Hadjem, A., Lacroux, F., Wong, M. F., & Wiart, J. (2008). Variability analysis of SAR from 20 MHz to 2.4 GHz for different adult and child models using finite-difference time-domain. *Physics in Medicine and Biology*, 53(6), 1511–1525. doi:10.1088/0031-9155/53/6/001 PMID:18367785
- Costa, C., Ferreira, C., Bastião, L., Ribeiro, L., Silva, A., & Oliveira, J. L. (2011). Dicoogle - an Open Source Peer-to-Peer PACS. *Journal of Digital Imaging*, 24(5), 848–856. doi:10.1007/s10278-010-9347-9 PMID:20981467
- El-Sharkawy, A.-M. M., Qian, D., Bottomley, P. A., & Edelstein, W. A. (2012). A multichannel, real-time MRI RF power monitor for independent SAR determination. *Medical Physics*, 39(5), 2334–2341. doi:10.1118/1.3700169 PMID:22559603
- Eurostat. (2019). *Healthcare resource statistics - technical resources and medical technology*. Retrieved from [https://ec.europa.eu/eurostat/statistics-explained/index.php/Healthcare\\_resource\\_](https://ec.europa.eu/eurostat/statistics-explained/index.php/Healthcare_resource_)
- Fiedler, T. M., Ladd, M. E., & Bitz, A. K. (2018). SAR Simulations & Safety. *NeuroImage*, 168, 33–58. doi:10.1016/j.neuroimage.2017.03.035 PMID:28336426
- Food and Drug Administration (FDA). (2014). *Criteria for Significant Risk Investigations of Magnetic Resonance Diagnostic Devices - Guidance for Industry and Food and Drug Administration Staff*. Retrieved from <https://www.fda.gov/regulatory-information/search-fda-guidance-documents/criteria-significant-risk-investigations-magnetic-resonance-diagnostic-devices-guidance-industry-and>
- Formica, D., & Silvestri, S. (2004). Biological effects of exposure to magnetic resonance imaging: An overview. *Biomedical Engineering Online*, 3(1), 11. doi:10.1186/1475-925X-3-11 PMID:15104797
- Hartwig, V. (2015). Engineering for safety assurance in MRI: Analytical, numerical and experimental dosimetry. *Magnetic Resonance Imaging*, 33(5), 681–689. doi:10.1016/j.mri.2015.02.001 PMID:25660641
- Hartwig, V., Tassano, S., Mattii, A., Vanello, N., Positano, V., Santarelli, M. F., Landini, L., & Giovannetti, G. (2013). Computational Analysis of a Radiofrequency Knee Coil for Low-Field MRI Using FDTD. *Applied Magnetic Resonance*, 44(3), 389–400. doi:10.1007/s00723-012-0388-8
- International Commission on Non-Ionizing Radiation Protection (ICNIRP). (2004). Medical magnetic resonance (MR) procedures: Protection of patients. *Health Physics*, 87(2), 197–216. doi:10.1097/00004032-200408000-00008 PMID:15257220
- Kalinowski, P., & Fidler, F. (2010). Interpreting Significance: The Differences Between Statistical Significance, Effect Size, and Practical Importance. *Newborn and Infant Nursing Reviews; NAINR*, 10(1), 50–54. doi:10.1053/j.nainr.2009.12.007
- Khalilzadeh, J., & Tasci, A. D. A. (2017). Large sample size, significance level, and the effect size: Solutions to perils of using big data for academic research. *Tourism Management*, 62(October), 89–96. doi:10.1016/j.tourman.2017.03.026

- Kim, S. J., & Kim, K. A. (2017). Safety issues and updates under MR environments. *European Journal of Radiology*, 89, 7–13. doi:10.1016/j.ejrad.2017.01.010 PMID:28267552
- Kraff, O., & Ladd, M. E. (2016). MR Safety Update 2015: Where Do the Risks Come From? *Current Radiology Reports*, 4(34), 1–7. doi:10.1007/s40134-016-0163-y
- Ma, W., Chen, L., Yang, Y., Zhou, Y., & Xu, B. (2016). Empirical analysis of network measures for effort-aware fault-proneness prediction. *Information and Software Technology*, 69, 50–70. doi:10.1016/j.infsof.2015.09.001
- Macbeth, G., Razumiejczyk, E., & Ledesma, R. D. (2011). Cliff's Delta Calculator: A non-parametric effect size program for two groups of observations. *Universitas Psychologica*, 10(2), 545–555. doi:10.11144/Javeriana.upsy10-2.cdcp
- Machata, A. M., Willschke, H., Kabon, B., Prayer, D., & Marhofer, P. (2009). Effect of brain magnetic resonance imaging on body core temperature in sedated infants and children. *British Journal of Anaesthesia*, 102(3), 385–389. doi:10.1093/bja/aen388 PMID:19174372
- Malik, S. J., Beqiri, A., Price, A. N., Teixeira, J. N., Hand, J. W., & Hajnal, J. V. (2015). Specific absorption rate in neonates undergoing magnetic resonance procedures at 1.5T and 3T. *NMR in Biomedicine*, 28(3), 344–352. doi:10.1002/nbm.3256 PMID:25594939
- Meliadò, E. F., van den Berg, C. A. T., Luijten, P. R., & Raaijmakers, A. J. E. (2019). Intersubject specific absorption rate variability analysis through construction of 23 realistic body models for prostate imaging at 7T. *Magnetic Resonance in Medicine*, 81(3), 2106–2119. doi:10.1002/mrm.27518 PMID:30414210
- Mugler, J. P. III. (2014). Optimized three-dimensional fast-spin-echo MRI. *Journal of Magnetic Resonance Imaging*, 39(4), 745–767. doi:10.1002/jmri.24542 PMID:24399498
- Nakaura, T., Kidoh, M., Maruyama, N., Kawahara, T., Namimoto, T., Sakai, Y., Harada, K., & Yamashita, Y. (2013). Usefulness of the SPACE pulse sequence at 1.5T MR cholangiography: Comparison of image quality and image acquisition time with conventional 3D-TSE sequence. *Journal of Magnetic Resonance Imaging*, 38(5), 1014–1019. doi:10.1002/jmri.24033 PMID:24105679
- National Electrical Manufacturers Association. (2019). *Digital Imaging and Communications in Medicine (DICOM) Standard: PS3.3 2019d - Information Object Definitions*. Retrieved from <https://www.dicomstandard.org/current/>
- Ono, A., Arao, S., Takata, S., Gotanda, T., Gotanda, R., & Tabuchi, A. (2019). Effect of Weight Input in Magnetic Resonance Imaging System on Radio-Frequency-Induced Heating of Metallic Implants. In L. Lhotska, L. Sukupova, I. Lacković, & G. S. Ibbott (Eds.), *World Congress on Medical Physics and Biomedical Engineering 2018* (pp. 11–14). Singapore: Springer Singapore. doi:10.1007/978-981-10-9038-7\_3
- Pianyhk, O. S. (2012). *Digital Imaging and Communications in Medicine (DICOM): A Practical Introduction and Survival Guide* (2nd ed.). Springer-Verlag Berlin Heidelberg. doi:10.1007/978-3-642-10850-1
- Qian, D., El-Sharkawy, A.-M., Bottomley, P., & Edelstein, W. (2013). An RF dosimeter for independent SAR measurement in MRI scanners. *Medical Physics*, 40(12), 122303. doi:10.1118/1.4829527 PMID:24320534
- Shah, N. J., Kaffanke, J. B., & Romanzetti, S. (2009). Repetition time and flip angle variation in SPRITE imaging for acquisition time and SAR reduction. *Journal of Magnetic Resonance (San Diego, Calif.)*, 199(2), 136–145. doi:10.1016/j.jmr.2009.01.036 PMID:19447652
- Shellock, F. G., & Crues, J. V. (2004). MR Procedures : Biologic Effects, Safety, and Patient Care. *Radiology*, 232(3), 635–652. doi:10.1148/radiol.2323030830 PMID:15284433
- Srinivasan, S., Kroeker, R. M., Gabriel, S., Plotnik, A., Godinez, S. R., Hu, P., Halnon, N., Finn, J. P., & Ennis, D. B. (2016). Free-Breathing Variable Flip Angle Balanced SSFP Cardiac Cine Imaging with Reduced SAR at 3T. *Magnetic Resonance in Medicine*, 76(4), 1210–1216. doi:10.1002/mrm.26011 PMID:26509846
- Stralka, J. P., & Bottomley, P. A. (2007). A Prototype RF Dosimeter for Independent Measurement of the Average Specific Absorption Rate (SAR) During MRI. *Journal of Magnetic Resonance Imaging*, 26(5), 1296–1302. doi:10.1002/jmri.21141 PMID:17969145

Tsai, L. L., Grant, A. K., Mortelet, K. J., Kung, J. W., & Smith, M. P. (2015). A Practical Guide to MR Imaging Safety: What Radiologists Need to Know. *Radiographics*, 35(6), 1722–1737. doi:10.1148/rg.2015150108 PMID:26466181

Wang, Z., & Collins, C. M. (2010). Effect of RF Pulse Sequence on Temperature Elevation for a Given Time-Average SAR. *Concepts in Magnetic Resonance. Part B, Magnetic Resonance Engineering*, 37B(4), 215–219. doi:10.1002/cmr.b.20172 PMID:21116480

## APPENDIX A

### Abbreviations Used in This Work

- .csv: comma-separated values
- $\mu$ s: microsecond
- BMI: body mass index
- cm: centimeter
- DICOM: Digital Imaging and Communications in Medicine
- Epi: echo planar imaging
- FDA: Food and Drug Administration
- FDTD: Finite Difference Time Domain
- Fid: free induction deca
- Flash: fast low angle shot
- FOV: field of view
- GRE: gradient ech
- Haste: half-Fourier acquisition single-shot turbo spin-echo
- ICNIRP: International Commission on Non-Ionizing Radiation Protection
- IEC: International Electrotechnical Commission
- IR: inversion recovery
- kg/m<sup>2</sup>: kilogram per square meter
- kg: kilogram
- <sup>MPRAGE</sup>: magnetization prepared rapid gradient echo
- MR: magnetic resonance
- mT/m: militesla per meter
- PACS: Picture Archiving and Communication Systems
- pSq: pulse sequence(s)
- RF: radiofrequency
- SAR: specific absorption rate
- SE: spin echo
- Space: sampling perfection with application optimized contrasts using different flip angle evolutions
- SpaceR: Space and RESTORE (trade name for a driven equilibrium (fast recovery) pulse);
- T/m/s: Tesla per meter per second
- T: tesla
- <sub>T1w</sub>: T1 weighted
- <sub>T2w</sub>: T2 weighted
- Tse: turbo spin echo
- W/kg: watts per kilogram
- $\delta$ : Cliff's delta

*Adriana Murraças is an early stage researcher in the field of medical imaging. She received a BSc in Biomedical Sciences in 2015 from University of Beira Interior and a MSc in Medical Imaging Technologies in 2017 from University of Aveiro. Her current research interests include magnetic resonance imaging, metadata management, statistical analysis issues and radiomics.*

*Paula Martins is Professor at the School of Health Sciences, University of Aveiro. She received a BSc in Radiography in 1987, a MSc in Speech and Hearing Sciences in 2007 and a PhD in Health and Technology Sciences in 2014, from University of Aveiro. She worked for 15 years as a Radiographer at Coimbra University Hospital. Her research interests include Speech Production, in particular Real time and Functional MRI applied to the study of Speech and Language. Additional interests include image processing and fine tuning of image acquisition protocols with an emphasis on image quality and patient radiation dose optimization. Paula Martins has been involved in different national research projects.*

*Carlos Daniel Cipriani Ferreira is an MRI Technologist and MRI Coordinator.*

*Tiago Marques Godinho has completed his Master's Degree in Computer and Telematics Engineering from the University of Aveiro in 2013. In the same year, he started the Computer Science PhD program. He was awarded a national scholarship for conducting his research on performance optimization in medical imaging information systems. Since then, he has published more than 6 articles in international peer-reviewed journals with impact factor and has participated in the fields major conferences. Last year, he completed his PhD program, and started a new challenge in the SW Engineering industry.*

*Augusto Marques Ferreira da Silva is an assistant professor at the Department of Electronics, Telecommunications and Informatics at the University of Aveiro. Research interests include medical image systems, medical image processing and imaging informatics.*